Detecting drones and human beings with DVB-S based COTS passive radar for short-range surveillance

Octavio Cabrera, Carlo Bongioanni, Francesca Filippini,
Olena Sarabakha, Fabiola Colone, Pierfrancesco Lombardo
DIET Dept., Sapienza University of Rome, Via Eudossiana, 18 - 00184 Rome, Italy
Email: octavio.cabrera@uniroma1.it

***Abstract*—This work addresses the exploitation of Digital Video Broadcasting - Satellite (DVB-S) signals as sources of opportunity for the surveillance of small targets in the proximity of critical infrastructures. A performance analysis has been carried out and it is reported to demonstrate the feasibility of the proposed system. Then, a preliminary experimental validation is performed using data collected by means of a low cost COTS based multi-polarimetric receiver to detect small and close targets, as drones and human beings. We present promising experimental results that show the capability of the proposed system to perform the desired task and, potentially, the opportunity to gain more information on the target motion based on its Doppler signature.**

***Index Terms*—Passive bistatic radar, DVB-S signal, COTS based, small target detections, polarimetric diversity**

I. Introduction

Passive bistatic radar (PBR) sensors [1] can detect and localize targets using signals emitted by non-cooperative sources, usually referred to as illuminators of opportunity (IOs). They are based on the bistatic radar technology, which consists of an emitter and a receiver that are not co-located.

In recent years, significant progress has been made in PBR technology and, depending on the considered application, different signals have been considered as sources of opportunity. Among them, a recently renewed interest has been received by the exploitation of satellite signals, such as GNSS (Global Navigation Satellite System) and DVB-S (Digital Video Broadcasting - Satellite), see e.g. [2]-[10] and the references therein. Among the main advantages of using this kind of signals, we recall their permanent world-wide availability as well as their wide transmitted bandwidth, which results in a good range resolution. Recently, some contributions have been published and have demonstrated the potential of satellite signals based PBR for a variety of applications. With particular reference to DVB-S signals, a waveform analysis has been reported in [11]; the authors in [4] showed the capability of such systems to detect ships, while the system feasibility for car detection was demonstrated in [10].

Nowadays, a challenging task is represented by the surveillance of critical infrastructures, that are potentially threatened by the intrusion of drones and unauthorized people, among others. For this reason, the purpose of this paper is to analyze the feasibility of polarimetric DVB-S based PBR for small target surveillance. Passive coherent location technology is particularly suitable for this task as it does not emit any electromagnetic radiation and thus it also allows covert operations.

The main contribution of this work is the preliminary demonstration of the possibility to perform the monitoring of small targets, drones and humans, in critical areas. To this aim, we develop a DVB-S based PBR demonstrator and we use it for an experimental validation.

The reminder of the paper is organized as follows. We introduce the system and its feasibility for the considered application in Section II. In Section III, we describe the acquisition campaign and the employed signal processing scheme. The experimental validation reported in Section IV shows the capability of the employed system to detect small targets. Finally, some conclusion remarks are reported in Section V.

II. DVB-S Based Passive Bistatic Radar

A typical PBR geometry is shown in Fig. 1. It includes two directional antennas, namely the reference antenna (R) pointed straight at the IO to collect the reference signal, and the surveillance antenna (S) steered toward the coverage area to collect target echoes.

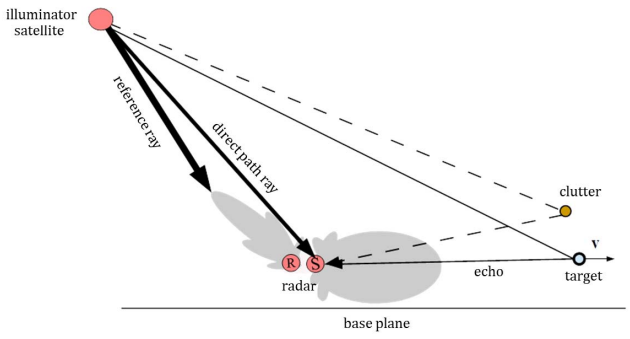

Fig. 1. Principal rays and antennas disposition.

978-1-7281-6813-5/20/$31.00 ©2020 IEEE

Several geostationary communication satellites are currently working and transmitting to Europe, specifically to Italy, with different equivalent isotropically radiated power (EIRP) values. Therefore, it is necessary to carry out a thorough investigation in order to find the best satellite with a good EIRP and a correct position, among other desirable parameters.

Once the satellite to be used has been selected, a performance prediction analysis must be carried out. In order to analyze the possibility to exploit DVB-S transmissions to detect targets, we use the well known bistatic radar equation to have a first approximation of the signal-to-noise ratio (SNR) level. The bistatic radar equation is given by

$$SNR = \frac{EIRP\ G\ c^2\sigma}{(4\pi)^3 f_0^2 d_E^2 d_T^2} \frac{T_i}{F k_B T} \tag{1}$$

being the employed parameters defined in Table I for the consider Astra 1M satellite and the receiving RF front-end developed for this project.

TABLE I
MAIN PARAMETERS OF EQ.(1)

PARAMETER	SYMBOL	VALUE
transmitted Power	EIRP	53 dBw
carrier frequency	f_0	10.7 GHz
emitter distance	d_E	36000 Km
receiver antenna S gain	G	5 dB
noise figure	F	1 dB
coherent processing interval	T_i	0.5s
Boltzmann constant	k_B	$1.38\ 10^{-23}$ J/K
light velocity	c	$3 \cdot 10^8$ m/s
Temperature	T	290 K

Fig. 2 shows the SNR as a function of d_T, which represents the distance from the transmitter to the target, for different values of σ, namely the target radar cross section (RCS). In this figure, we consider very short distances, relevant for the surveillance application under analysis.

As an example, we use the Albersheim's equation [12], denoting P_{fa} and P_d as the false alarm and detection probabality, respectively. Accordingly, for a $P_d = 0.8$ and a $P_{fa} = 10^{-4}$, we obtain a required target SNR (SNR_T) of 12 dB. For this example, looking at Fig. 2, we see that a target with a $\sigma = 0.01$ m^2 could be detected up to a distance of $d_T = 10$ m, while a target with $\sigma = 0.1$ m^2 is in principle visible up to $d_T = 30$ m. Notice that the origin of the short-range limitation is not only the small RCS of the target, but also the low gain in the S antenna. Specifically, for this performance prediction, we used a 5 dB gain antenna, which allows us to have a wide angular coverage.By considering a standard DVB-S bandwidth of $\Delta B = 30$ MHz for each channel, the resulting bistatic range resolution (ΔR_B) and the resulting Doppler frequency (Δf_D) are 7 m and 2 Hz, respectively [1].

III. EXPERIMENTAL CAMPAIGN

In this section we explain the architecture of the RF front-end based on commercial off-the-shelf (COTS) components. As is represented in Fig. 3, we use a parabolic reflector for the reference antenna, and only a small feedhorn for the surveillance antenna. In order to have two cross-polarizations in the reference parabolic reflector we install a small feedhorn antenna with an orthomode transducer (OMT) in the focus of the reflector (see Fig. 4). In the same way an OMT is installed in the surveillance feedhorn (see Fig. 5).

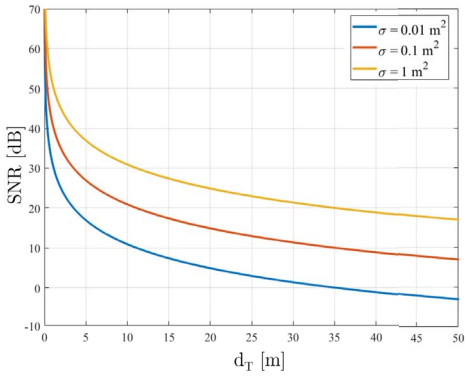

Fig. 2. The SNR as a function of d_T for different values of σ.

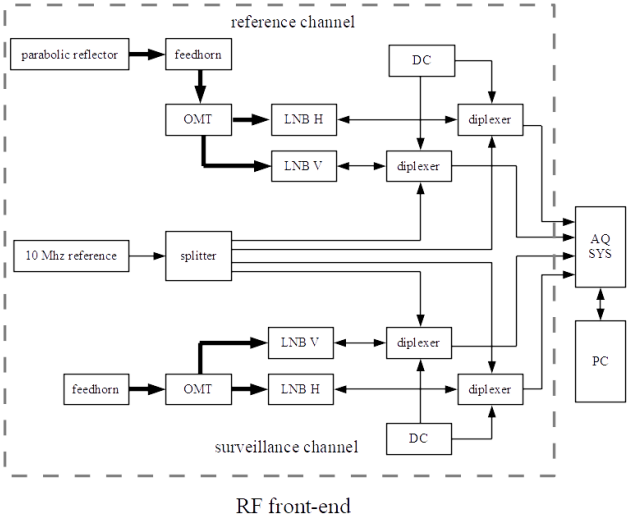

Fig. 3. Block diagram of the RF front-end architecture. Thicker lines represent wave-guides connections while simple lines wire connections.

The OMT has two outputs, each one is connected to an low noise block (LNB), which allows us to take the signal in Ku band and shift it to L band. Since each LNB needs to share the same connector to receive a 10 MHz reference signal, the direct current (DC) source and the output in the L band, we used a diplexer circuit, whose output is the signal in the L band. Note that the 10 MHz reference signal for the four LNBs ensures the coherence between the different channels. Finally, the four channels are digitized in the L band in the acquisition system (AQ SYS). The components used in the demonstrator are summarized in Table II.

Let us consider the general case of a DVB-S based PBR receiver, equipped with P differently polarized surveillance channels. First, the available surveillance signals are separately

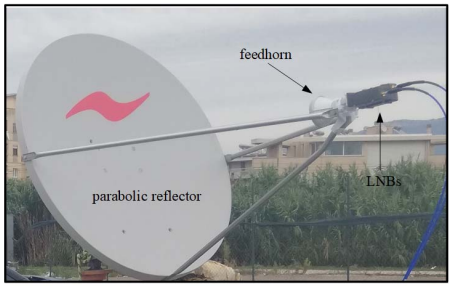

Fig. 4. Reference antenna with a parabolic reflector, a feedhorn, an OMT and two LNBs.

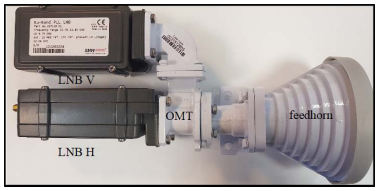

Fig. 5. Surveillance antenna with a feedhorn, an OMT and two LNBs.

TABLE II
USED COMPONENTS FOR THE RF FRONT-END

COMPONENT	MODEL
parabolic reflector	SKYWARE 96cm
feed	SKYWARE for 96 cm antenna
AQ SYS	NI USRP-2955
LNB	SMW Ku Band LNB
diplexer	SMW diplexer with 10 MHz ref. input

processed according to the main stages of a conventional passive radar processing scheme, sketched in Fig. 6. Afterwards, the P outputs are jointly exploited for target detection purposes.

Specifically, as Fig. 6 shows, the first processing step is the disturbance cancellation stage. It aims at reducing the Direct Path Signal (DPS) contribution, as well as strong clutter and multipath. To this purpose, we use the extensive cancellation algorithm - batch (ECA-B), proposed in [13] and based on subtracting the undesired interference signal, estimated by summing up delayed and weighted replicas of the reference signal, from the surveillance channel. By recalling that the length of the frames L sets the range of bistatic velocities that will be filtered together with the clutter and DPS, we used frames of length $L = 2 \cdot 10^6$ samples. The P outputs of this disturbance cancellation stage are then used to evaluate the cross ambiguity function (CAF) to obtain one bistatic range - Doppler map for each polarimetric channel, say $\psi(f_D, R_B)_p, p = 0, ..., P-1$, where (f_D, R_B) represents the generic Doppler and range pair. In this work, we perform the CAF evaluation using the batch algorithm method [14], with a CPI $T_i = 0.5s$.

IV. EXPERIMENTAL VALIDATION

In this section, we prove the feasibility of the proposed system against real data. To this aim, a dedicated acquisition

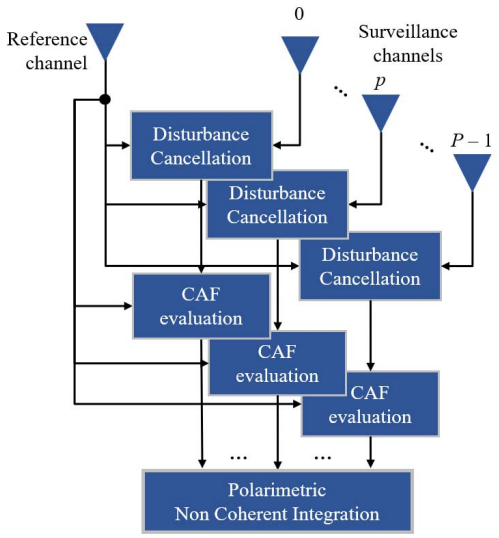

Fig. 6. Signal processing scheme.

campaign has been carried out in a parking area at Cisterna di Latina, Italy. The acquisition geometry is sketched in Fig.7. Two different data sets have been collected, one using a small drone as cooperative target and the other aimed at detecting a moving human being. The signal processing scheme described in section III has been applied to the two different data sets and the results are separately reported in the following subsections.

A. Results against drone

In order to investigate the capability to detect small drones, a DJI Mavic Pro has been used as cooperative target, flying away from the receiver up to approx. 25 m (see the red line in Fig.7). First, in Fig. 8 (a-b), we compare the results obtained for one datafile, say datafile #1, by separately using vertical (V) and horizontal (H) polarization, respectively, for a CPI of 0.5s. In the same way, in Fig. 9 (a-b) we show the results obtained for another time window of the same size, say datafile #2. Each figure represents the test statistic over the bistatic range-Doppler plane before the detection stage, mapped into the nominal P_{fa} that would allow the corresponding threshold exceeding. In other words, each pixel has been scaled to represent the minimum value of nominal P_{fa} to be set for that pixel to yield a detection.

Figs. 8 and 9 confirm what has been demonstrated in [15], [16], namely that depending on the complex structure of the target, the signal polarization may change in the reflection. In fact, the target echo at the two cross-polarized channels does not appear as an equally strong peak. Specifically, when datafile #1 is considered, the H channel (Fig. 8 (a)) would be able to detect the drone for very low values of desired P_{fa}, while the V channel (Fig. 8 (b)) only receives a weak echo from that target, i.e. a very high P_{fa} would be necessary for it to be detected. An opposite behavior is observed datafile #2 (see Fig. 9 (a-b)) where the V polarized channel (Fig. 9 (b))

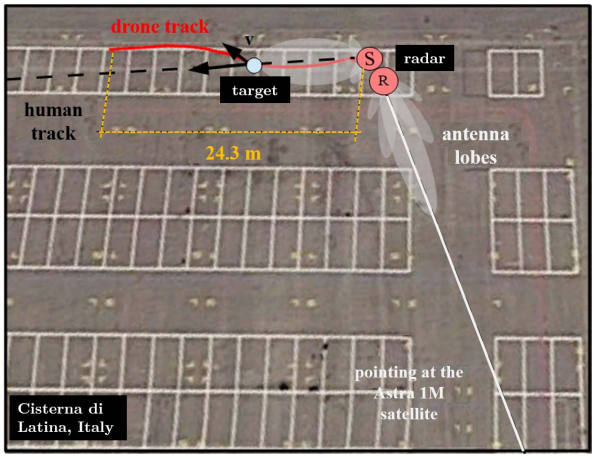

Fig. 7. Acquisition geometry.

is the best performing one. Therefore, Figs. 8 and 9 show that it is hard to a priori establish which is the best performing single polarized channel.

For this reason, the signals collected by the two cross-polarimetric channels are jointly exploited, i.e. $P = 2$ (H and V), and a non coherent integration (NCI) is performed accross the polarimetric dimension, as follows

$$\psi_{NCI}(f_D, R_B) = |\psi(f_D, R_B)_V|^2 + |\psi(f_D, R_B)_H|^2 \quad (2)$$

The $\psi_{NCI}(f_D, R_B)$ for the two considered cases are reported in Fig.8 (c) and Fig.9 (c). They show that using the NCI approach, we are always able to recover the target echo with respect to the single polarized cases.

Once the described stages have been applied, the target detection stage is performed. In particular, when each polarimetric channel is separately considered, i.e. $P = 1$, the detection stage is performed by directly applying a cell average - constant false alarm rate (CA-CFAR) threshold to the resulting map in order to detect targets with a given P_{fa}. We will refer to this scheme as the conventional single-pol operation in the following. In contrast, when $P = 2$, the CA-CFAR is applied on the integrated range-velocity map. We will refer to this approach as polarimetric NCI in the following. Further details are reported in [15], [16].

In both cases, the detection threshold is properly selected in order to obtain a desired false alarm rate, based on the following expression [15]

$$P_{fa} = \sum_{p=0}^{P-1} \binom{PM+p-1}{p} \left(\frac{\gamma}{PM}\right)^p \left(1+\frac{\gamma}{PM}\right)^{-PM-p} \quad (3)$$

where γ represents the threshold and M denotes the employed number of training data for the noise floor estimation.

In Fig.10 we report the raw detections obtained for the 40 consecutive datafiles as gray plots in a common bistatic range-Doppler plane, for $P_{fa} = 10^{-4}$. The different gray shades map the temporal information, starting from the darkest one. In particular, Fig.10 (a) and (b) show the results obtained using the H and V polarization, respectively, while Fig.10 (c) shows the results obtained using the polarimetric NCI approach. Fig.10 confirms the considerations made on Figs. 8 and 9 and shows that, using the proposed solution, we are able to detect the drone with a good continuity for its entire trajectory.

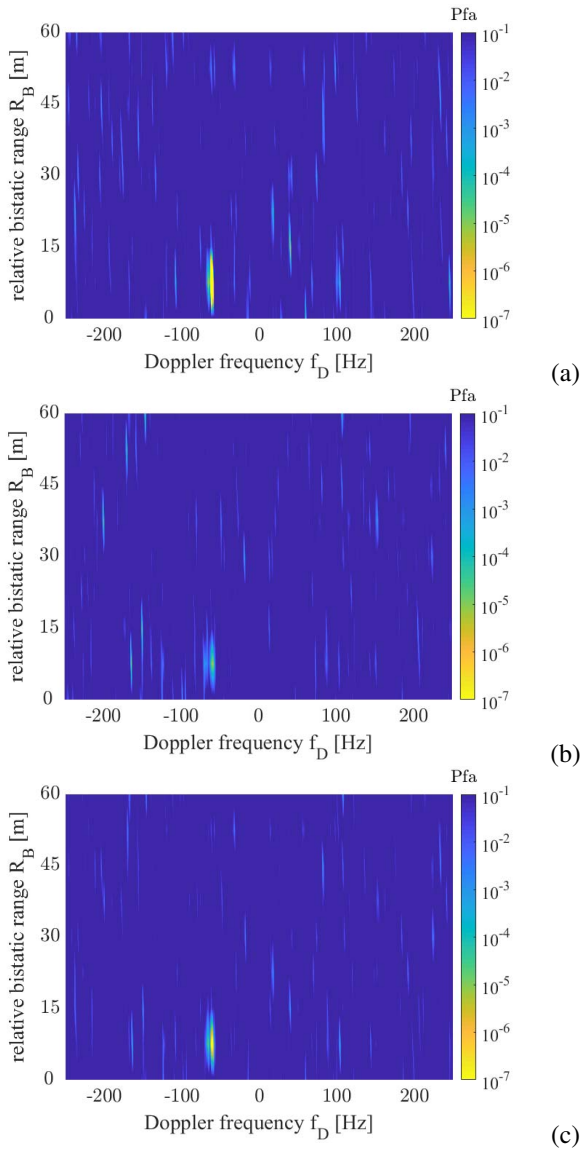

Fig. 8. Results against drone for datafile #1: Minimum nominal P_{fa} values in the range-Doppler domain to be set in order to detect each bin, using (a) single-pol H (b) single-pol V (c) polarimetric NCI.

B. Results against human target

The human movement has also been analyzed. To this aim, we performed an experiment where a human target was running away from the surveillance antenna (see dashed black line in Fig7). In Fig. 11 (a-b) we show the function $\psi_{NCI}(f_d, R_B)$ obtained for two single datafiles with a CPI of

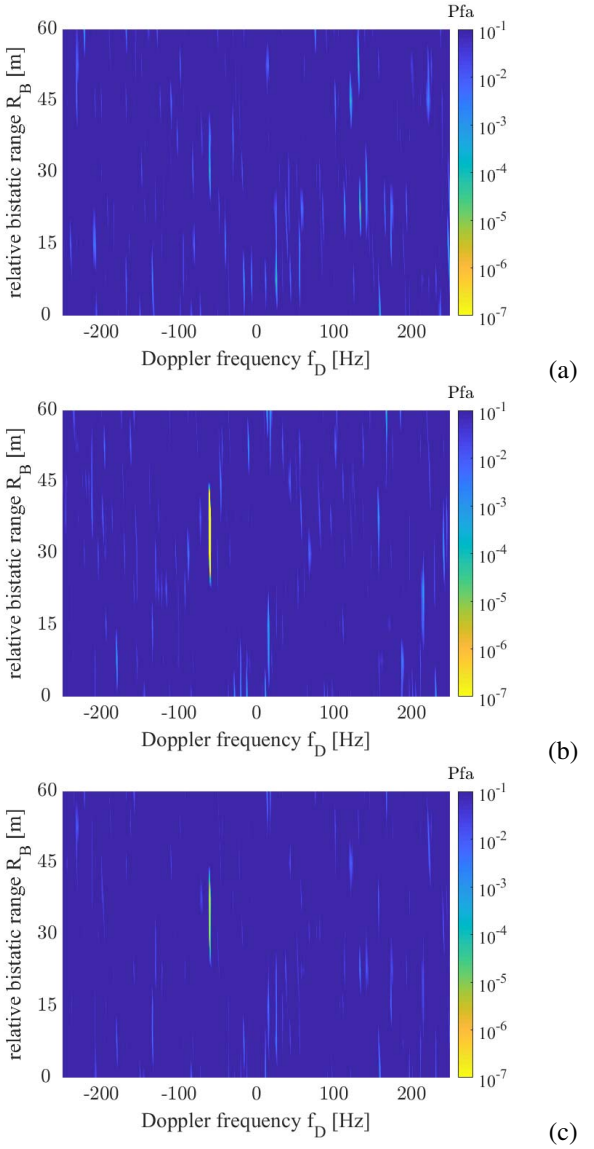

Fig. 9. Results against drone for datafile #2: Minimum nominal P_{fa} values in the range-Doppler domain to be set in order to detect each bin, using (a) single-pol H (b) single-pol V (c) polarimetric NCI.

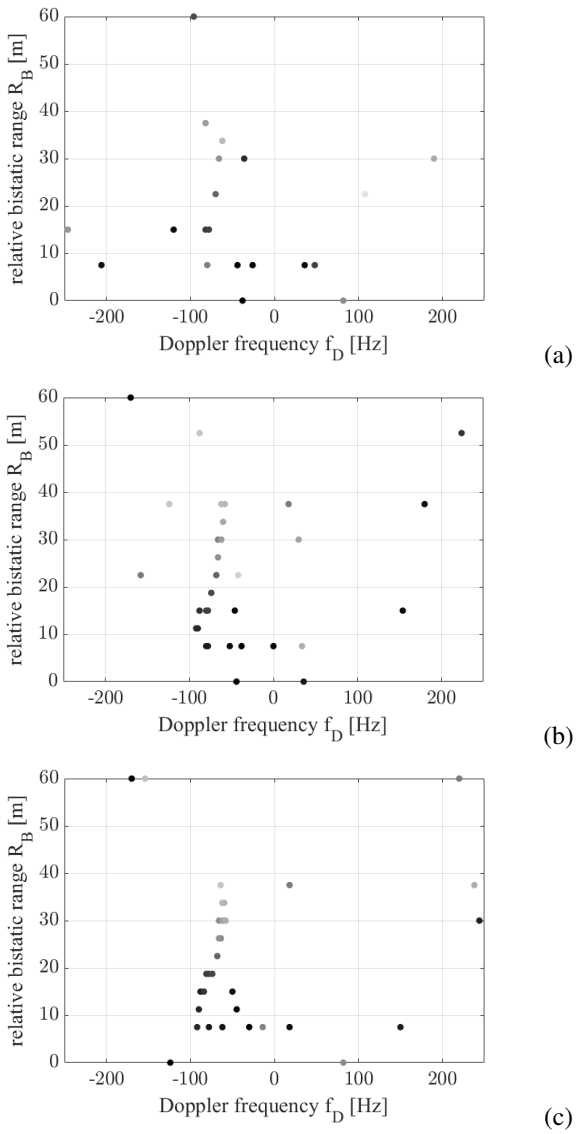

Fig. 10. Results against drone: Raw detections for 40 consecutive data windows with $P_{fa} = 10^{-4}$, using (a) single-pol H (b) single-pol V (c) polarimetric NCI. Different gray shades map the temporal information, starting from the darkest one.

0.5s, extracted at the time when the human was starting its run (a) and at the time he was running quickly (b). In both cases, the target peak is approx. 20dB above the disturbance power level. Incidentally, note that this result matches with the SNR analysis reported in Fig. 2 for a RCS of 1 m^2, which is likely to correspond to the monostatic RCS of a human [17]. Moreover, it is evident that along with the mass center that was moving with an approx. constant velocity, the limbs were also fluctuating, resulting in the insurgence of the micro-Doppler phenomena. This is particularly evident in Fig. 11 (b) and could potentially allow us to infer on the type of target movement, via a classification based on the different micro-Doppler signatures. Clearly, Fig. 11 (b) also suggests that a proper selection of the training data to be used in the CA-CFAR detection stage must be carried out. In Fig. 11 (c), we show the detection results obtained for the human target for a set of 40 consecutive datafiles with $P_{fa} = 10^{-6}$, using training data selected only in the range dimension in order to avoid including micro-Doppler contributions in the secondary cells. Furthermore, to face the problem of having multiple detections in the Doppler domain at each range bin we only considered one detection per range cell, using the detections center of gravity. Using these strategies, the human trajectory can be easily identified in Fig. 11 (c).

V. Conclusion

The feasibility of passive radar systems based on DVB-S opportunity transmissions for the detection of small targets

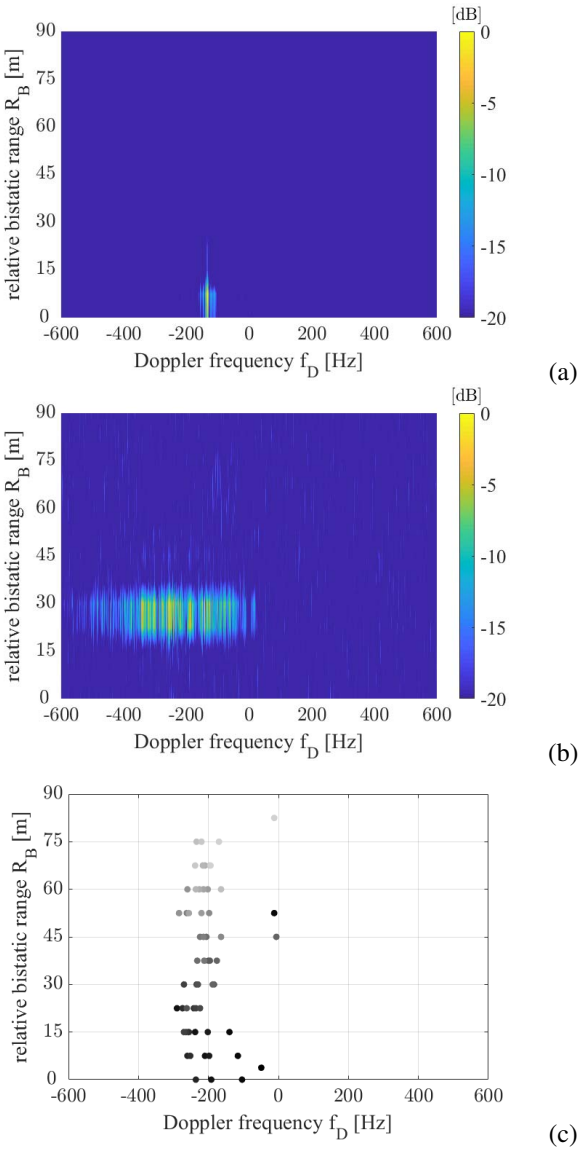

Fig. 11. Results against human target : (a)-(b) $\psi_{NCI}(f_D, R_B)$ obtained for two different datafiles (c) human path detections for 40 consecutive datafiles with $P_{fa} = 10^{-6}$. Different gray shades map the temporal information, starting from the darkest one.

(drones and humans) has been preliminarly demonstrated. To this aim, an experimental analysis has been carried out. Furthermore, it has been proven that a big parabolic reflector is not necessary to detect small targets at very short ranges. In this work, a simple feedhorn with approximately 5 dB gain has been used. This approach also allowed to achieve wide angular coverage. This work also demonstrates that the joint exploitation of different polarimetric channels according to the polarimetric NCI can effectively improve the performance of the system with respect to the use of single polarimetric channels. It is expected that higher gain antennas will enable the detection of small targets at higher distances. Future works will include a performance assessment in longer range surveillance applications as well as the employment of the developed RF front-end architecture to localize the detected targets. Moreover, advance signal processing strategies to exploit polarization diversity will be considered with the purpose of further improving the performance while different solution to extract the micro-Doppler signatures will be investigated.

VI. Acnowledgement

The authors gratefully acknowledge Genex RF s.r.l. for the valuable advices regarding the RF components selection.

References

[1] H. D. Griffiths and C. J. Baker, *Introduction to Passive Radar*, Norwood, MA, USA: Artech, Mar. 2017.

[2] D. Pastina et al., "Maritime Moving Target Long Time Integration for GNSS-Based Passive Bistatic Radar," in *IEEE Transactions on Aerospace and Electronic Systems*, vol. 54, no. 6, pp. 3060-3083, Dec. 2018.

[3] J. -L. Bárcena-Humanes, N. del-Rey-Maestre, M. P. Jarabo-Amores, D. Mata-Moya and P. Gomez-del-Hoyo, "Passive radar imaging capabilities using space-borne commercial illuminators in surveillance applications," *2015 Signal Processing Symposium (SPSympo)*, Debe, 2015, pp. 1-5.

[4] L. Daniel, S. Hristov, X. Lyu, A. G. Stove, M. Cherniakov and M. Gashinova, "Design and Validation of a Passive Radar Concept for Ship Detection Using Communication Satellite Signals," in *IEEE Transactions on Aerospace and Electronic Systems*, vol. 53, no. 6, pp. 3115-3134, Dec. 2017.

[5] H. Nies, F. Behner, S. Reuter and O. Loffeld, "First Results of Passive Radar Imaging and Tracking Using Geostationary Satellites," *2018 15th European Radar Conference (EuRAD)*, Madrid, 2018, pp. 214-217.

[6] I. Pisciottano, D. Cristallini and D. Pastina, "Maritime target imaging via simultaneous DVB-T and DVB-S passive ISAR," in *IET Radar, Sonar and Navigation*, vol. 13, no. 9, pp. 1479-1487, 9 2019.

[7] A. G. Stove, M. S. Gashinova, S. Hristov and M. Cherniakov, "Passive Maritime Surveillance Using Satellite Communication Signals," in *IEEE Transactions on Aerospace and Electronic Systems*, vol. 53, no. 6, pp. 2987-2997, Dec. 2017.

[8] D. Cristallini, M. Caruso, P. Falcone, D. Langellotti, C. Bongioanni, F. Colone, S. Scafè, P. Lombardo, "Space-Based Passive Radar Enabled By The New Generation Of Geostationary Satellites", *IEEE Aerospace Conference*, Big Sky (MT), USA, 6-13 March 2010.

[9] A. Arcangeli, C. Bongioanni, N. Ustalli, D. Pastina, P. Lombardo, "Passive Forward Scatter Radar based on satellite TV broadcast for air target detection: preliminary experimental results", *IEEE Radar Conference* 2017, 9-11 May 2017, Seattle, WA (USA).

[10] P. Gomez-del-Hoyo, M. Jarabo-Amores, D. Mata-Moya, N. del-Rey-Maestre and J. Rosado-Sanz, "First Approach on Ground Target Detection with GPS based Passive Radar: Experimental Results," *2019 Signal Processing Symposium (SPSympo)*, Krakow, Poland, 2019, pp. 71-75.

[11] Z. Sun, T. Wang, T. Jiang, C.Chen and W. Chen, "Analysis of the properties of DVB-S signal for passive radar application," *2013 International Conference on Wireless Communications and Signal Processing, Hangzhou, 2013, pp. 1-5.*

[12] W. J. Alberhseim, "A closed-form approximation to Robertson's detection characteristics," in in *Proceedings of the IEEE*, vol. 69, no. 7, pp. 839-839, July 1981.

[13] F. Colone, D. W. O'Hagan, P. Lombardo and C. J. Baker, "A Multistage Processing Algorithm for Disturbance Removal and Target Detection in Passive Bistatic Radar," in *IEEE Transactions on Aerospace and Electronic Systems*, vol. 45, no. 2, pp. 698-722, April 2009.

[14] P. Lombardo and F. Colone, " Advanced processing methods for passive bistatic radar', in Melvin, W. L., and Scheer, J. A. (Eds.): 'Principles of Modern Radar: Advanced Radar Techniques', Raleigh, NC: SciTech Publishing, 2012, pp. 739–821.

[15] F. Colone and P. Lombardo, "Polarimetric passive coherent location," in *IEEE Transactions on Aerospace and Electronic Systems*, vol. 51, no. 2, pp. 1079-1097, April 2015.

[16] F. Filippini, F. Colone, D. Cristallini and G. Bournaka, "Experimental results of polarimetric detection schemes for DVB-T-based passive radar," in *IET Radar, Sonar and Navigation*, vol. 11, no. 6, pp. 883-891, 6 2017.

[17] M.A. Richards, Fundamentals of Radar Signal Processing, McGraw-Hill Companies, New York (2005).